*The American Journal of Pathology, Vol. 176, No. 4, April 2010*

*DOI: 10.2353/ajpath.2010.090561*

*Tumorigenesis and Neoplastic Progression*

# *Ricinus communis* Agglutinin I Leads to Rapid Down-Regulation of VEGFR-2 and Endothelial Cell Apoptosis in Tumor Blood Vessels

Weon-Kyoo You,* Ian Kasman,*
Dana D. Hu-Lowe,† and Donald M. McDonald*

*From the Cardiovascular Research Institute,* Comprehensive Cancer Center, and Department of Anatomy, University of California, San Francisco, California; and the Department of Research Pharmacology,† Pfizer Global Research and Development, San Diego, California*

***Ricinus communis* agglutinin I (RCA I), a galactose-binding lectin from castor beans, binds to endothelial cells at sites of plasma leakage, but little is known about the amount and functional consequences of binding to tumor endothelial cells. We addressed this issue by examining the effects of RCA I on blood vessels of spontaneous pancreatic islet-cell tumors in RIP-Tag2 transgenic mice. After intravenous injection, RCA I bound strongly to tumor vessels but not to normal blood vessels. At 6 minutes, RCA I fluorescence of tumor vessels was largely diffuse, but over the next hour, brightly fluorescent dots appeared as the lectin was internalized by endothelial cells. RCA I injection led to a dose- and time-dependent decrease in vascular endothelial growth factor receptor-2 (VEGFR-2) immunoreactivity in tumor endothelial cells, with 95% loss over 6 hours. By comparison, VEGFR-3, CD31, and CD105 had decreases in the range of 21% to 33%. Loss of VEGFR-2 was followed by increased activated caspase-3 in tumor vessels. Prior inhibition of VEGF signaling by AG-028262 decreased RCA I binding and internalization into tumor vessels. These findings indicate RCA I preferentially binds to and is internalized by tumor endothelial cells, which leads to VEGFR-2 down-regulation, endothelial cell apoptosis, and tumor vessel regression. Together, the results illustrate the selective impact of RCA I on VEGF signaling in tumor blood vessels.** ***(Am J Pathol 2010, 176:1927–1940; DOI: 10.2353/ajpath.2010.090561)***

Tumor vessels are irregularly shaped and tortuous, and have multiple functional abnormalities.[1–3] Endothelial cells comprising tumor vessels have abnormalities in gene expression, require growth factors for survival, and have defective barrier function to plasma proteins.[1,3] Molecules that are preferentially expressed on tumor vessels can serve as therapeutic targets.[2]

Plant lectins have been used to characterize the surface properties of cells and to isolate membrane proteins of endothelial cells.[4–8] *Ricinus communis* agglutinin (RCA I, RCA 120) and *Ricinus communis* toxin (ricin, RCA II, RCA 60) are galactose-binding lectins from seeds of the castor bean plant *R. communis*.[9–13] Both lectins bind to erythrocytes and endothelial cells *in vitro*,[14–16] but the effects are strikingly different. RCA I is a potent galactoside-binding lectin and hemagglutinin, and ricin is a potent enzymatically active toxin.[11]

RCA I and ricin are heterodimeric proteins with two components. RCA I consists of two A chains and two B chains, and ricin has one A and one B chain joined by a single disulfide bridge.[9–13] The sequence of the A and B chains of RCA I and ricin have homologies but are not identical.[12] The A chain of RCA I and ricin is cytotoxic because its glycosidase activity inactivates ribosomal protein synthesis; the B chain is a lectin that mediates endocytosis by binding galactosyl and *N*-acetylgalactosaminyl residues of cell surface glycoconjugates.[12,13] However, ricin ($LD_{50}$ 5 to 36 $\mu$g/kg in mice) is much more toxic than RCA I ($LD_{50}$ ~1400 $\mu$g/kg).[17,18] A single molecule of enzymatically active ricin A chain reportedly can inactivate 1500 ribosomes per minute, inhibit protein synthesis, and cause cell death.[13] Because of this activity, ricin has been used as a biological weapon and as an immunotoxin for cancer therapeutics.[13,19–23] Effects of ricin by endothelial cells may result in the vascular leak

Supported in part by National Institutes of Health grants HL24136 and HL59157 from the National Heart, Lung, and Blood Institute, CA82923 from the National Cancer Institute, funding from AngelWorks Foundation (to D.M.), and by the Korea Research Foundation Grant No. M01-2004-000-20020-0 (to W.-K.Y.).

Accepted for publication December 11, 2009.

Current address of W.-K.Y. Sanford-Burnham Medical Research Institute, La Jolla, CA; of I.K., Genentech Inc., South San Francisco, CA.

Address reprint requests to Donald M. McDonald, M.D., Ph.D., Department of Anatomy, University of California, 513 Parnassus Avenue, Room S1363, San Francisco, CA 94143-0452. E-mail: donald.mcdonald@ucsf.edu.

syndrome found with immunotoxins or other therapeutics containing ricin A chain.[24–27]

Studies of lectins injected into the vasculature have shown that RCA I, unlike *Lycopersicon esculentum* (LEA, tomato lectin), does not bind uniformly to the luminal surface of the endothelium, but instead binds preferentially to leaky sites in the endothelium of inflamed venules.[7] RCA I also binds to the luminal surface of endothelial cells of murine squamous carcinomas, indicative of affinity for tumor blood vessels,[28] and to sinusoidal endothelial cells of liver and bone marrow[29] and certain other vessels.[30]

To obtain a better understanding of the selectivity and functional consequences of RCA I binding to endothelial cells of tumor blood vessels *in vivo*, we examined the distribution of rhodamine-labeled RCA I in tumors after i.v. injection into RIP-Tag2 transgenic mice that have spontaneous pancreatic islet cell adenomas and carcinomas. Using immunohistochemistry and fluorescence and confocal microscopy, we found that rhodamine-RCA I bound much more strongly to tumor vessels than to normal blood vessels of the surrounding acinar pancreas. The lectin initially coated much of the luminal surface of tumor vessels but after an hour had a conspicuous dot-like pattern, indicative of internalization into endosomes and lysosomes of endothelial cells. Vascular endothelial growth factor (VEGF) receptor (R)-2 immunoreactivity of endothelial cells subsequently decreased, endothelial cells underwent apoptosis, and tumor vessels regressed. These findings demonstrate that RCA I can selectively reduce VEGFR-2 in endothelial cells of tumor blood vessels *in vivo*.

## Materials and Methods

### Animals and Treatment

Spontaneous pancreatic islet cell carcinomas in RIP-Tag2 mice (C57BL/6 background) were studied at 10 to 11 weeks of age.[31] All experimental procedures were reviewed and approved by the University of California, San Francisco Institutional Animal Care and Use Committee. AG-028262, a potent small molecule inhibitor of VEGFR tyrosine kinases, supplied by Pfizer Global Research and Development (San Diego, CA), or vehicle was administered to some mice once daily for 7 days by gavage (80 mg/kg/dose in a volume of 5 $\mu$l/g).[32]

### Lectin Injection and Fixation by Vascular Perfusion

For assessment of RCA I binding to tumor blood vessels, RIP-Tag2 mice were injected with rhodamine-labeled RCA I lectin (Vector Laboratories, RL-1082)[33,34] into a tail vein in doses ranging from 0.5 to 500 $\mu$g. The time course of lectin-mediated effects was examined at 6 minutes, 1 hour, or 6 hours after injection of 500 $\mu$g RCA I or at 24 hours after injection of 5 $\mu$g or 50 $\mu$g RCA I. Dose-dependency was examined at 6 hours after injection of 0.5, 5, 50, or 500 $\mu$g RCA I. Fluorescein isothiocyanate (FITC)-labeled LEA lectin (Vector Laboratories, FL-1171) was injected into some mice to assess patency of tumor vessels.[32,33]

At the end of the experiment, mice were anesthetized with ketamine (83 mg/kg) plus xylazine (13 mg/kg, i.m.). The chest was opened rapidly, and the vasculature was perfused with fixative (1% paraformaldehyde in PBS, pH 7.4) for 2 minutes at a pressure of 120 mmHg from an 18-gauge cannula inserted into the aorta via an incision in the left ventricle. Blood and fixative exited through an opening in the right atrium. The entire pancreas with tumors and multiple normal organs (kidney, liver, spleen, thyroid, trachea) were removed and immersed in fixative for 1 hour at 4°C. Specimens were rinsed with PBS, infiltrated with 30% sucrose in PBS overnight at 4°C, embedded in optimal cutting temperature compound (Sakura Finetek), and frozen at −20°C.

### Immunohistochemistry

Endothelial cells of tumor vessels were stained by immunohistochemistry using our previously described methods[32–34] with one or more antibodies: rat anti-mouse CD31 (PECAM-1, clone MEC 13.3, 1:500; BD Pharmingen), hamster anti-mouse CD31 (clone 2H8, 1:500; Chemicon), rabbit anti-mouse VEGFR-2 (TO14, 1:2000; gift from Rolf Brekken, University of Texas Southwestern Medical Center), goat anti-mouse VEGFR-3 (1:1000; R&D Systems), or rat anti-mouse CD105 (endoglin, clone MJ7/18, 1:500; BD Pharmingen). VEGF was stained with goat anti-mouse VEGF-A (anti-VEGF, 1:50; R&D systems). Macrophages were stained with rat anti-F4/80 (1:250; Serotec). Apoptotic cells were labeled with rabbit anti-human/mouse activated caspase-3 (1:1000; R&D Systems).

Secondary antibodies (1:400; Jackson ImmunoResearch Laboratories Inc.) included FITC- or Cy5-labeled goat or donkey anti-rat or hamster IgG; FITC-, Cy3 or Cy5-labeled goat anti-rabbit IgG; FITC-labeled donkey anti-goat IgG; FITC- or Cy3-labeled donkey anti-goat IgG.

### Fluorescence Imaging

Tissue sections were examined with a Zeiss Axiophot fluorescence microscope equipped with single, dual, and triple fluorescence filters and a CCD camera (CoolCam, SciMeasure; 640 × 480-pixel RGB-color images) and with a Zeiss LSM 510 confocal microscope with Argon, Helium-Neon, and UV lasers (512 × 512- or 1024 × 1024-pixel RGB-color images).

### Measurements of Tumor Vascularity and Rhodamine-RCA I Fluorescence

RCA I fluorescence and immunofluorescence of various markers in tumors were quantified by measuring the proportion of sectional area (area density) occupied by the fluorescence above the threshold intensity.[32–34] Digital fluorescence microscopic images, each representing a region measuring 960 × 1280 $\mu$m, were captured from

sections of at least four tumors in each RIP-Tag2 mouse. Images were analyzed using ImageJ software (*http://rsb.info.nih.gov/ij; 1.32j*). Based on an analysis of pixel fluorescence intensities, which ranged from 0 to 255, specific staining was distinguished from background by empirically using a threshold value of 50. Area density of VEGFR-2, VEGFR-3, CD31, CD105, or activated caspase-3 immunofluorescence and RCA I or LEA lectin was calculated as the proportion of pixels having a fluorescence intensity value equal to or greater than the threshold.[32–34] Area density of VEGFR-2 or CD31 immunoreactivity in acinar pancreas was determined in the same manner.

### *Measurement of Rhodamine-RCA I in Peripheral Blood*

The concentration of rhodamine-RCA I was measured in 100 $\mu$l of blood withdrawn from the tail vein at 3 minutes, 10 minutes, 30 minutes, 1 hour, or 6 hours after intravenous (iv) injection of 500 $\mu$g of RCA I into RIP-Tag2 mice.[35] Plasma was obtained by centrifugation of whole blood at 4000 rpm for 15 minutes. The concentration of RCA I in plasma was measured by spectrofluorometry (SPECTRAmax, Gemini, Molecular Devices), based on standard solutions prepared from RCA I at an initial concentration of 250 $\mu$g/ml diluted with the plasma from control mice. Total blood volume of mice was estimated to be 80 ml/kg.[36,37]

### *RCA I-Binding to VEGFR-2 in Tumors*

To estimate RCA I-binding to VEGFR-2, biotinylated RCA I (500 $\mu$g/mouse, Vector Laboratories, B-1085) or vehicle was injected into a tail vein of RIP-Tag2 mice and allowed to circulate for 1 hour. After perfusion with PBS, tumors were removed and homogenized in radioimmunoprecipitation assay buffer (50 mmol/L Tris-Cl, pH 7.4, 150 mmol/L NaCl, 1% NP-40, 0.5% deoxycholate, 0.1% SDS). After centrifugation, the supernatant (100 $\mu$g of protein) was incubated with avidin agarose resin (Pierce) for 16 hours at 4°C, and then the precipitant was washed five times with radioimmunoprecipitation assay buffer containing 0.5 mol/L NaCl. After centrifugation and resuspension in SDS sample buffer (62.5 mmol/L Tris-Cl, pH 6.8, 10% glycerol, 2% SDS, 0.01% bromphenol blue), the precipitant was analyzed on 4% to 20% Tris-Glycine gels (Invitrogen) and then transferred to nitrocellulose membranes (Amersham Pharmacia Biotech). The gel was stained by Coomassie Blue to detect proteins in the precipitant. To identify VEGFR-2 in the precipitant, the membranes were incubated in PBS containing 5% bovine serum albumin and 0.05% Tween 20 and then incubated with rabbit anti-VEGFR-2 (TO14). Proteins in the precipitants, which bound with anti-VEGFR-2, were detected by using enhanced chemiluminescence reagents (Pierce). VEGFR-2 identified by immunoprecipitation, using anti-VEGFR-2 (TO14) and rabbit anti-mouse/rat VEGFR-2 (Flk-1, C-20, Santa Cruz), on tumor homogenates from RIP-Tag2 mice without injection of biotinylated RCA I, was used as a positive control.

### *$LD_{50}$ of RCA I in RIP-Tag2 Mice*

To determine the $LD_{50}$ of RCA I (lethal dose for 50% of RIP-Tag2 mice), 25, 50 or 500 $\mu$g RCA I was injected by tail vein and the duration of survival was determined ($n$ = 5 mice/dose). $LD_{50}$ of RCA I was calculated by the method reported by Zhan and Zhou.[18] A plot of dose/survival time versus dose gave a straight line, with the $y$-intercept of the equation equal to the $LD_{50}$ value.[18]

### *Colocalization of Activated Caspase-3 and CD31*

The amount of colocalization of activated caspase-3 with CD31 immunoreactivity was measured on fluorescence microscopic images of sections of RIP-Tag2 tumors. Digital images of the red channel (activated caspase-3 labeled with Cy3-conjugated secondary antibody) and green channel (CD31 labeled with FITC-conjugated secondary antibody) of the same field were captured separately with the CCD camera. The colocalized pixels were identified by using the colocalization plug-in function of ImageJ.[34]

### *Isosurface Rendering of Confocal Images*

Confocal RGB image stacks were imported into Imaris software (version 5.0.3; Bitplane). Voxels with fluorescence intensities above a threshold were assigned to each color channel. Isosurfaces were rendered from these voxels and smoothed with a Gaussian filter, creating three-dimensional reconstructions in which the spatial resolution was conserved.[38]

### *Measurements of Internalized RCA I*

Fluorescence dots, representing internalized RCA I in endosomes or lysosomes in endothelial cells of tumor vessels, were counted in confocal microscopic images. Each confocal image stack (×40 objective, ×3 zoom) represented a region measuring 76.8 × 76.8 $\mu$m and a thickness of 40 $\mu$m. Images were captured from sections of at least four tumors in each mouse. RCA I fluorescent dots were counted in five randomly positioned boxes (0.5 × 0.5 $\mu$m) over tumor vessels of each image.

### *Statistics*

The significance of differences between groups was assessed using analysis of variance (ANOVA) followed by the Bonferroni-Dunn test for multiple comparisons. Values are expressed as means ± SE ($n$ = 4 to 5 mice per group). $P$ values less than 0.05 were considered significant.

## Results

### Preferential Binding of Rhodamine-RCA I to Tumor Blood Vessels

After i.v. injection of rhodamine-RCA I, the vasculature of RIP-Tag2 tumors had intense red fluorescence, but blood vessels of the surrounding acinar pancreas had little or none (Figure 1A). Indeed, tumors were conspicuous because their bright red fluorescence sharply contrasted with the surrounding nonfluorescent tissue (Figure 1A). Most RCA I colocalized with tumor vessels marked by VEGFR-2 immunoreactivity; vessels in the acinar pancreas had little or no red fluorescence (Figure 1, B and C). The brightness of RCA I in tumor vessels varied from intense to faint (Figure 1, D and E).

The area density of RCA I fluorescence was 15% in RIP-Tag2 tumors but only 0.6% in the surrounding acinar pancreas (Figure 1F). RCA I fluorescence was detected in some veins of the liver (Figure 1G) and most renal glomeruli (Figure 1H), but the intensity was much fainter than that of tumor vessels. Little or no RCA I fluorescence was found in the spleen, acinar pancreas, thyroid, or trachea.

### Internalization of Rhodamine-RCA I by Endothelial Cells of Tumor Vessels

The largely diffuse red fluorescence of tumor vessels present at 6 minutes after injection of RCA I was distinctly punctate at 1 hour (Figure 1, I and J). This time-dependent change in distribution of RCA I fits with surface clustering or internalization into endosomes or lysosomes of endothelial cells, as is well documented for internalization of VEGF/VEGFR-2 complexes into endothelial cells *in vitro*.[39–42]

To learn more about whether the dot-like pattern of red fluorescence reflected internalization of RCA I, we compared the distribution of VEGF and VEGFR-2 immunoreactivities in tumor vessels. As expected from *in vitro* studies,[39–42] both VEGF and VEGFR-2 had dot-like patterns in endothelial cells similar to the punctate RCA I fluorescence (Figure 1, K and L), and most of the punctate VEGF colocalized with VEGFR-2 (Figure 1L, arrowheads).

### Time Course of Internalization of RCA I

The patterns of RCA I labeling (red) and VEGFR-2 immunoreactivity (green) of tumor vessels underwent conspicuous changes from 6 minutes to 6 hours after injection of the lectin (Figure 2, A–E). At 6 minutes, tumor vessels had a subtle pattern of small red dots superimposed on diffuse red fluorescence of RCA I and prominent generalized green fluorescence of VEGFR-2 immunoreactivity (Figure 2, A and D).

At 1 hour, RCA I had more conspicuous dot-like fluorescence, but VEGFR-2 staining was about the same (Figure 2, B and E). Most punctate red fluorescence of RCA I colocalized with identical green dots of VEGFR-2 immunoreactivity assumed to be endosomes or lysosomes (Figure 2, F, and G, arrows), but some dots of RCA I did not have VEGFR-2 immunoreactivity (Figure 2, F, and G, arrowheads).

At 6 hours, the red fluorescence of RCA I and green fluorescence of VEGFR-2 were strikingly different from 1 hour. Neither RCA I nor VEGFR-2 showed the pattern of tumor vessels (Figure 2, C, H, and I). Instead, both RCA I and VEGFR-2 colocalized in blobs as large as 10 $\mu$m in the region of tumor vessels, but the vascular pattern was indistinct or absent (Figure 2, H and I).

Measurements of the plasma concentration in peripheral blood of RIP-Tag2 mice from 3 minutes to 6 hours after i.v. injection of 500 $\mu$g RCA I gave a calculated half-life of 8 minutes (Figure 2J). RCA I concentration in plasma was 167 $\mu$g/ml at 3 minutes after injection and was 25 $\mu$g/ml at 6 hours (Figure 2J).

Because of the colocalization of RCA I with VEGFR-2, we sought to determine whether RCA I also colocalizes with VEGF by comparing the distribution of RCA I to the corresponding distributions of VEGF immunoreactivity. Most dot-like objects of RCA I fluorescence did not colocalize with dot-like VEGF immunoreactivity in RIP-Tag2 tumor vessels (Figure 3, A–D). The tumor vessels dominant by RCA I dots had fewer VEGF dots and vice versa (Figure 3, A–D).

### RCA I Binding to VEGFR-2 in Tumors

To determine whether the colocalization of RCA I and VEGFR-2 immunoreactivity reflected binding to VEGF receptors, we injected biotinylated RCA I (500 $\mu$g) as a probe and then analyzed RIP-Tag2 tumor homogenates by avidin-agarose precipitation and VEGFR-2 immunoprecipitation. Biotinylated-RCA I protein complexes in avidin precipitants prepared from tumors 1 hour after injection of biotinylated lectin had a mobility of 220 kDa on SDS-polyacrylamide electrophoresis gel (Figure 3E, lane 1). Western blots of biotinylated RCA I-injected tumor homogenates stained with anti-VEGFR-2 antibody showed a clear band for VEGFR-2 at 220 kDa (Figure 3F, lane 1). Tumor homogenates from mice injected with vehicle gave no signal at 220 kDa on SDS-polyacrylamide electrophoresis gel (Figure 3E, lane 2) or Western blot (Figure 3F, lane 2) after avidin agarose precipitation. VEGFR-2 immunoprecipitation of tumor homogenates showed an intense signal close to 220 kDa (Figure 3F, lane 3) but no protein band on SDS-polyacrylamide electrophoresis gel (Figure 3E, lane 3).

### Reduction in VEGFR-2 after RCA I: Selectivity

To determine whether the striking decrease of VEGFR-2 immunoreactivity of tumor vessels after injection of RCA I was due to a selective effect on VEGFR-2 or to a generalized action of RCA I on protein synthesis,[12,17,18] we asked whether similar changes occurred in other endothelial cell membrane proteins, VEGFR-3, CD31, and CD105.

The strong VEGFR-2 immunoreactivity of tumor vessels present at 6 minutes after injection of RCA I (Figure 4A)

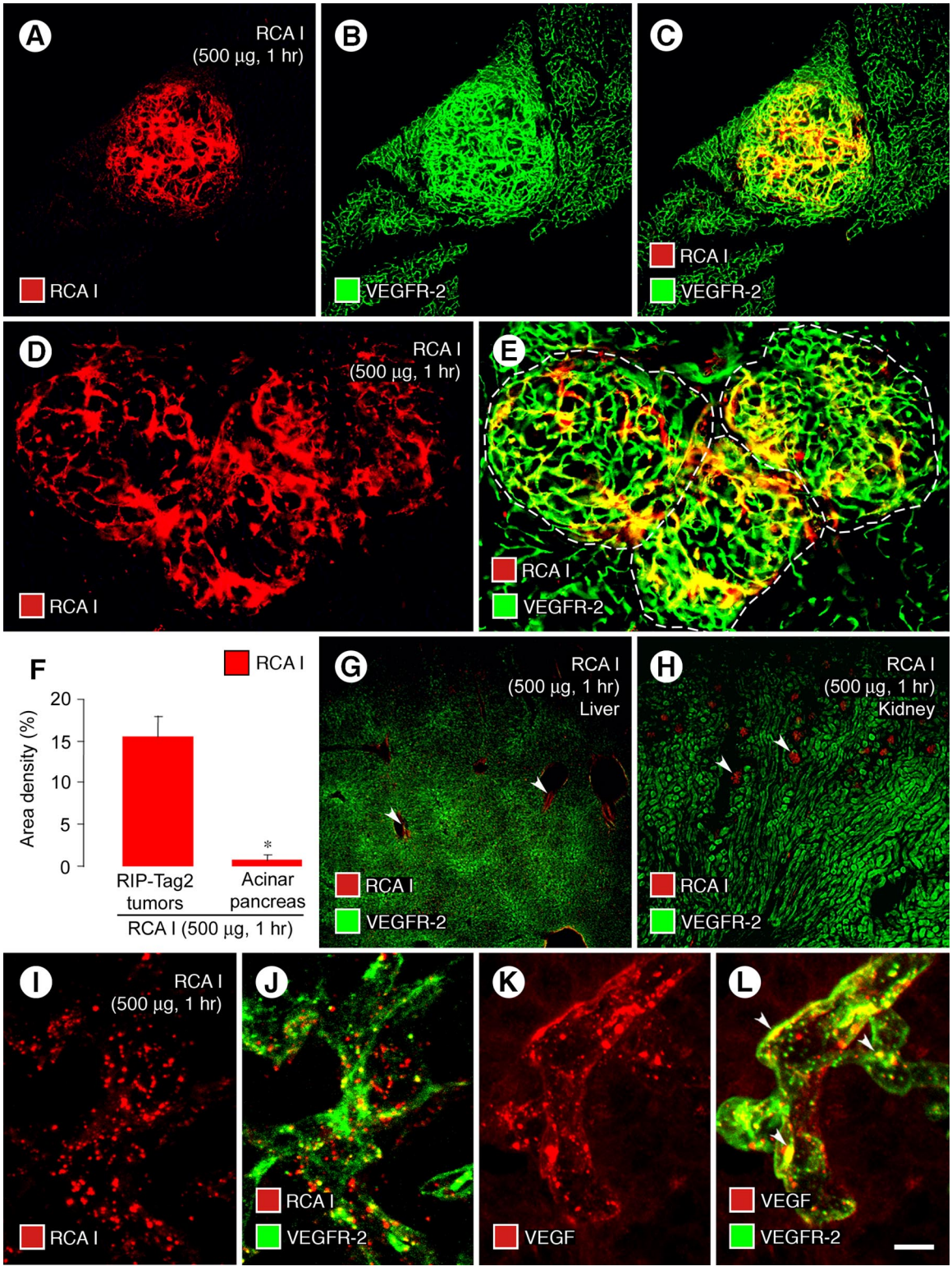


**Figure 1.** Preferential binding and internalization of RCA I by tumor vessels. Micrographs of RIP-Tag2 tumors (**A**–**C**) showing strong red fluorescence of tumor vessels 1 hour after i.v. injection of 500 $\mu$g rhodamine-RCA I and green VEGFR-2 immunofluorescence. Strong red fluorescence of tumor vessels (**D, E, dashed lines** outline tumors) contrasts with little or no fluorescence of blood vessels in surrounding acinar pancreas. Bar graph (**F**) compares abundant RCA I fluorescence (fractional area, 15%) of tumor vessels with almost no fluorescence (0.6%) in the acinar pancreas. Micrographs show weak RCA I fluorescence in central veins of the liver (**G**, **arrowheads**) and glomeruli of the kidney (**H**, **arrowheads**). Confocal micrographs show dot-like red fluorescence of RCA I that colocalizes with green VEGFR-2 immunofluorescence in endothelial cells of tumor vessels (**I**, **J**; 1 hour after injection of rhodamine-RCA I). Confocal images of tumor vessels show the dot-like pattern of VEGF immunoreactivity (**K**), most of which colocalizes with green VEGFR-2 immunofluorescence (**L**, **arrowheads**). $^*P < 0.05$ compared with value for tumors (**F**). Scale bar in (**L**)**:** 240 $\mu$m (**A**–**C**, **G**, **H**); 120 $\mu$m (**D**, **E**); 10 $\mu$m (**I**–**L**).

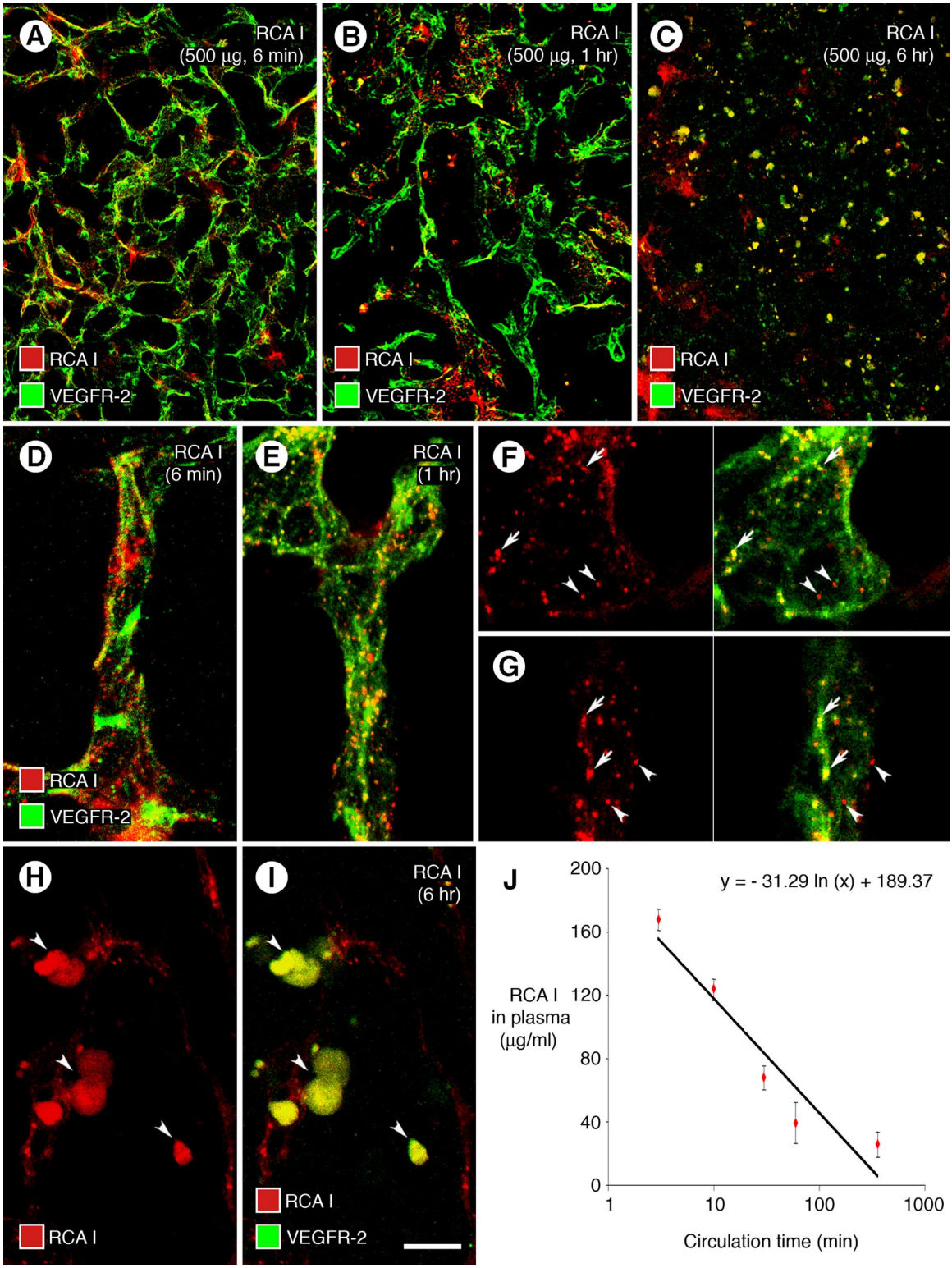


**Figure 2.** Distribution of RCA I binding and internalization in tumors. Confocal micrographs compare the distribution of red fluorescence in RIP-Tag2 tumors at 6 minutes, 1 hour, or 6 hours after i.v. injection of 500 $\mu$g rhodamine-RCA I (**A**–**C**). RCA I fluorescence had diffuse, patchy pattern at 6 minutes (**A**), dot-like pattern at 1 hour (**B**), and blob-like pattern at 6 hours (**C**), when VEGFR-2 immunoreactivity changed from faithful marking of tumor vasculature to blobs (**C**). RCA I and VEGFR-2 were largely separate at 6 minutes (**D**), but colocalized in some dot-like (endosomes) at 1 hour (**E**, yellow-green). Colocalization of RCA I and VEGFR-2 was clear in some endosomes viewed in individual optical sections of confocal stack images (**F**, **G**, **arrows**) but was not present in others at 1 hour (**F**, **G**, **arrowheads**). At 6 hours, most colocalized RCA I and VEGFR-2 fluorescence in tumors was in the form of blobs, and VEGFR-2 no longer marked tumor vessels (**H**, **I**, **arrowheads**). RCA I in plasma had a half-life of 8 minutes (**J**) and a concentration of 25.2 $\mu$g/ml at 6 hours after injection (**J**). Scale bar in (**I**): 90 $\mu$m (**A**–**C**); 15 $\mu$m (**D**–**E**, **H**–**I**); 10 $\mu$m (**F**–**G**).

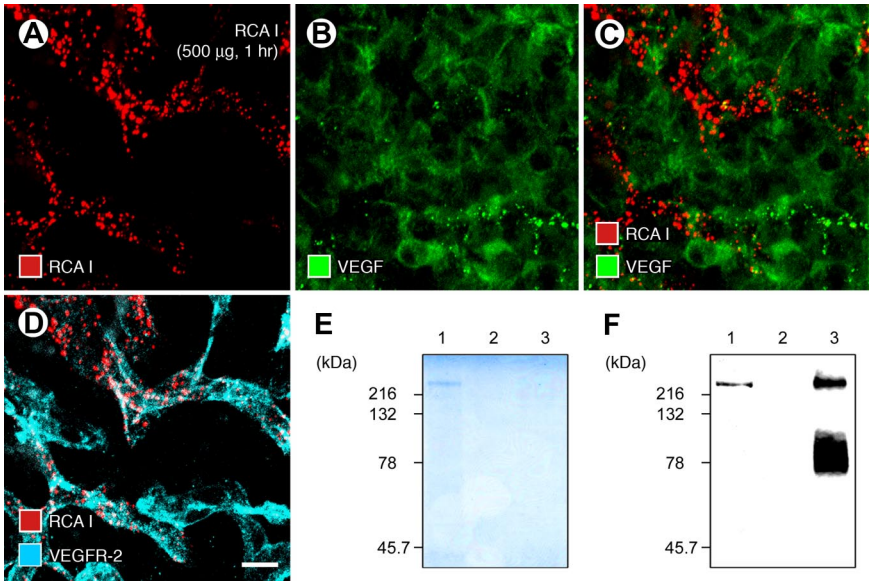


**Figure 3.** RCA I association with VEGFR-2 but not with VEGF. Confocal micrographs show the mutually exclusive distributions of dot-like red fluorescence of RCA I (500 μg, 1 hour) and green immunofluorescence of VEGF in RIP-Tag2 tumors (**A**–**C**). By comparison, some RCA I co-localized with VEGFR-2 (**D**). Scale bar in (**D**): 10 μm (**A**–**D**). SDS- polyacrylamide electrophoresis gel (**E**) showing clear protein staining for avidin agarose precipitants of biotinylated RCA I-protein complexes at 220 kDa (**E**, **lane 1**) in RIP-Tag2 tumor homogenates 1 hour after injection of 500 μg biotinylated RCA I. No protein band was detected in avidin agarose precipitants of tumor homogenates in the absence of biotinylated RCA I (**E**, **lane 2**) or in VEGFR-2 immunoprecipitation fractions of RIP-Tag2 tumor homogenates (**E**, **lane 3**). Western blots (**F**) of tumor homogenates showing a weak but distinct band for VEGFR-2 (**F**, **lane 1**) after injection of biotinylated RCA I, no VEGFR-2 band (**F**, **lane 2**) without biotinylated RCA I, and intense bands (**F**, **lane 3**) of VEGFR-2 immunoprecipitation.

but was markedly reduced at 6 hours (Figure 4B), when the fractional area of staining was 95% less than baseline (Figure 4C). By comparison, VEGFR-3 immunoreactivity, which was strong on tumor vessels (Figure 4D), was reduced by only 21% at 6 hours (Figure 4, E and F). VEGFR-3 staining was not present on blood vessels of the acinar pancreas but was strong on peritumoral lymphatics (Figure 4D, arrowheads), which was not reduced by RCA I (Figure 4E, arrowheads). CD31 staining of tumor vessels, which was initially strong (Figure 4G), was reduced by 27% at 6 hours (Figure 4, H and I). CD105 (endoglin) immunoreactivity was present on many tumor vessels (Figure 4J) and was reduced by 33% at 6 hours after RCA I (Figure 4, K and L).

## *Reduction in VEGFR-2 after RCA I: Dose-Dependence*

The reduction of VEGFR-2 immunoreactivity of tumor vessels after RCA I was dose-dependent. VEGFR-2 staining was not noticeably reduced at 6 hours after a dose of 0.5 μg but was conspicuously lower after 50 μg (Figure 5, A and B). Measurements showed a reduction of 85% after a dose of 50 μg and 95% after 500 μg (Figure 5, C–E). Changes in VEGFR-2 were significantly greater than the reductions in CD31 (Figure 5E), which was reduced by 30% at 6 hours after a dose of 50 μg and by 39% after 500 μg (Figure 5E).

Corresponding changes in blood vessels of the acinar pancreas were significantly lower than in tumor vessels (Figure 5, F and G). VEGFR-2 immunoreactivity of acinar pancreas blood vessels was not reduced at 6 hours after RCA I at a dose of 0.5 or 5 μg but was reduced by 55% after a dose of 50 μg and by 86% after 500 μg (Figure 5F). CD31 staining of acinar pancreas vessels was reduced by 21% at 6 hours after a dose of 50 μg and by 24% after 500 μg (Figure 5F). Many tumor vessels that had strong CD31 immunoreactivity at 6 hours after 50 μg of RCA I lacked VEGFR-2 immunoreactivity (Figure 5H, and I, arrowheads).

## *Reduction in VEGFR-2 after RCA I: Progressive Effects*

Injection of a relatively low dose RCA I (5 μg), which had no noticeable effect at 6 hours, caused conspicuous changes in tumor vessels at 24 hours. In these mice, VEGFR-2 immunoreactivity of tumor vessels was strikingly reduced (Figure 5, J and K), but CD31 staining showed little change (Figure 5L).

In addition, doses of RCA I greater than 25 μg were lethal in RIP-Tag2 mice, and the duration of survival was dose-dependent (Figure 5M). Mice lived an average of 21 hours after a dose of 5 μg, 14.5 hours after 50 μg, and 9.5 hours after 500 μg. From the dose/survival data, the $LD_{50}$ of RCA I in RIP-Tag2 mice was calculated as 1.23 mg/kg (Figure 5M).

## *Tumor Vessel Regression after RCA I*

To determine whether the profound reduction of VEGFR-2 immunoreactivity was accompanied by diminished vessel function,[43] we assessed vessel patency and perfusion by i.v. injection of FITC-labeled LEA lectin, which binds uniformly and rapidly to the luminal surface of blood vessels.[32,33] When 500 μg of RCA I was injected 1 hour before the LEA lectin, the pattern of LEA staining matched the distribution of tumor vessels revealed by CD31 staining (Figure 6A). However, when RCA I was injected 6 hours before the LEA lectin, fewer tumor vessels were stained by LEA than were evident from CD31 immunoreactivity (Figure 6B, arrowheads). The fractional area of tumor vessels stained by LEA at 6 hours after RCA I was 53% less than at 1 hour (Figure 6C). This mismatch reflects the loss of patency before vessel regression.[33]

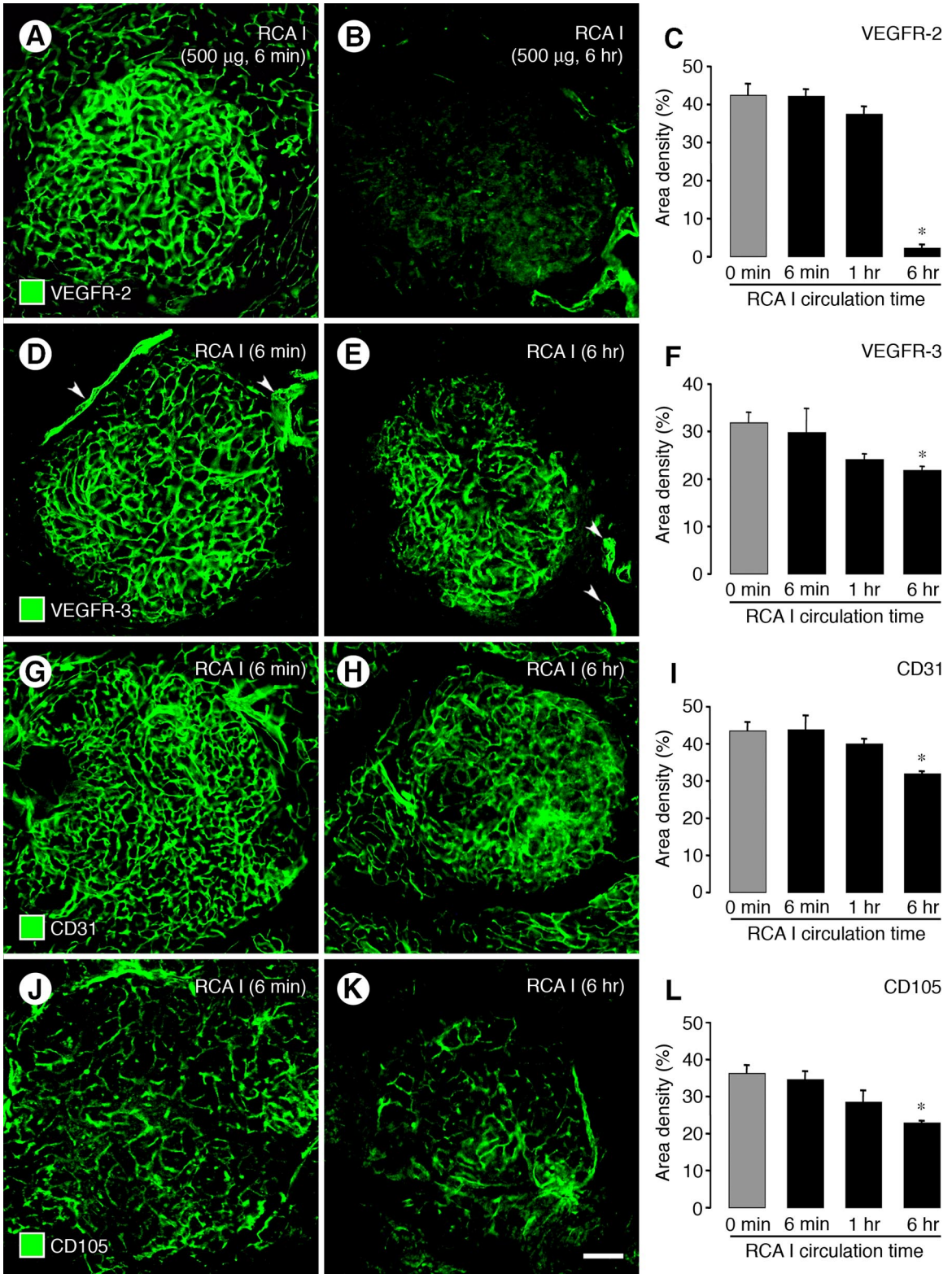


**Figure 4.** Comparison of RCA I effects on VEGFR-2 with other membrane proteins. Fluorescence micrographs comparing changes in VEGFR-2 with corresponding changes in VEGFR-3, CD31, and CD105 immunoreactivities of tumor vessels at 6 minutes and 6 hours after i.v. injection of 500 μg RCA I. VEGFR-2 immunoreactivity was strong at 6 minutes but markedly reduced at 6 hours (**A**, **B**). Measurements revealed that the reduction in VEGFR-2 at 6 hours was 95% (**C**). By comparison, at 6 hours VEGFR-3 in tumor vessels was reduced only 21% (**D**–**F**), CD31 was reduced 27% (**G**–**I**), and CD105 was reduced 30% (**J**–**L**). However, VEGFR-3 immunoreactivity was still strong in peritumoral lymphatics at 6 hours after RCA I (**D**, **E**, **arrowheads**). VEGFR-3 and CD105 were stronger in tumor vessels than in vessels of the surrounding acinar pancreas (**D**–**E**, **J**–**K**). *$P < 0.05$ compared with 0 minutes (no RCA I) in all graphs. Scale bar in (**K**)**:** 120 μm (all micrographs).

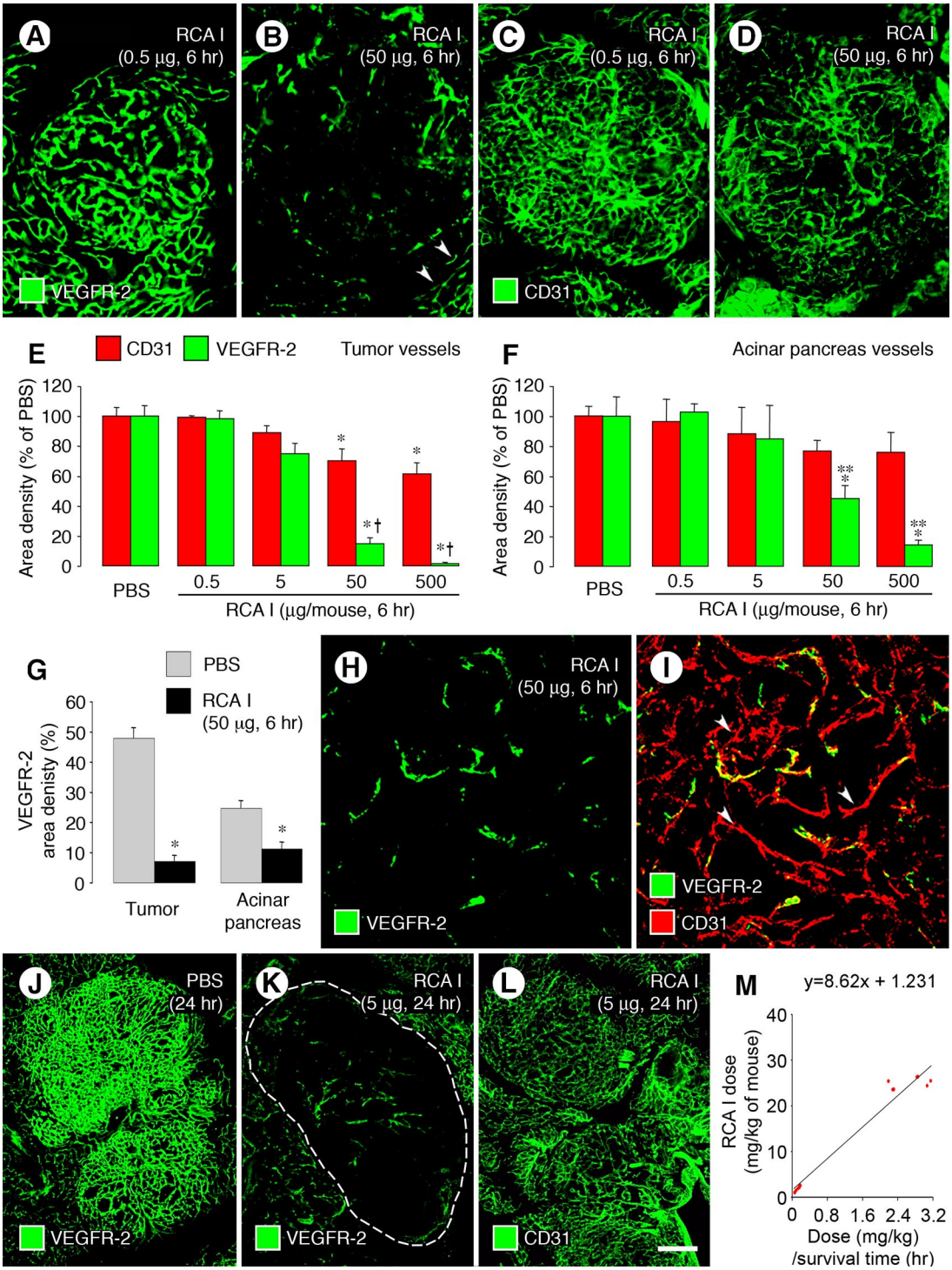


**Figure 5.** Dose- and time-dependency of VEGFR-2 reduction after RCA I. Fluorescence micrographs and graphs showing the dose-dependent reduction in VEGFR-2 immunoreactivity of tumor blood vessels at 6 hours after injection of RCA I (**A**–**F**). VEGFR-2 in tumor vessels did not change after RCA I at a dose of 0.5 $\mu$g but tended to be lower after 5 $\mu$g, and was significantly reduced after 50 or 500 $\mu$g. VEGFR-2 in blood vessels of acinar pancreas (**B**, **arrowheads**) also decreased with the higher doses but the reductions were smaller than in tumor vessels (**E**, **F**). Reductions in CD31 immunoreactivity were smaller than VEGFR-2, both in tumor vessels (**E**) and acinar pancreas vessels (**F**). The reduction of VEGFR-2 in tumor vessels at 6 hours after 50 $\mu$g RCA I was significantly larger than the corresponding change in blood vessels of acinar pancreas (**G**). Despite the striking reduction in VEGFR-2 immunoreactivity in tumors at 6 hours, the vasculature could still be identified by staining for CD31 (**H**, **I**, **arrowheads**), indicating that the vessels were still present. When tumor vessels were assessed at 24 hours after the injection, a 5-$\mu$g dose of RCA I markedly reduced VEGFR-2 immunoreactivity (**J**, **K**, **dashed lines** outlines tumor) but not CD31 immunoreactivity (**L**). Plot of RCA I dose (mg/kg)/survival time versus RCA I dose in RIP-Tag2 mice (**M**). The *y*-intercept gives an $LD_{50}$ of 1.23 mg/kg in mice.[18] $^{*}P < 0.05$ compared with PBS group in all graphs; $^{**}P < 0.05$ compared with value for CD31 (**E**–**F**). Scale bar in (**L**)**:** 120 $\mu$m (**A**–**D**); 60 $\mu$m (**H**, **I**); 240 $\mu$m (**J**–**L**).

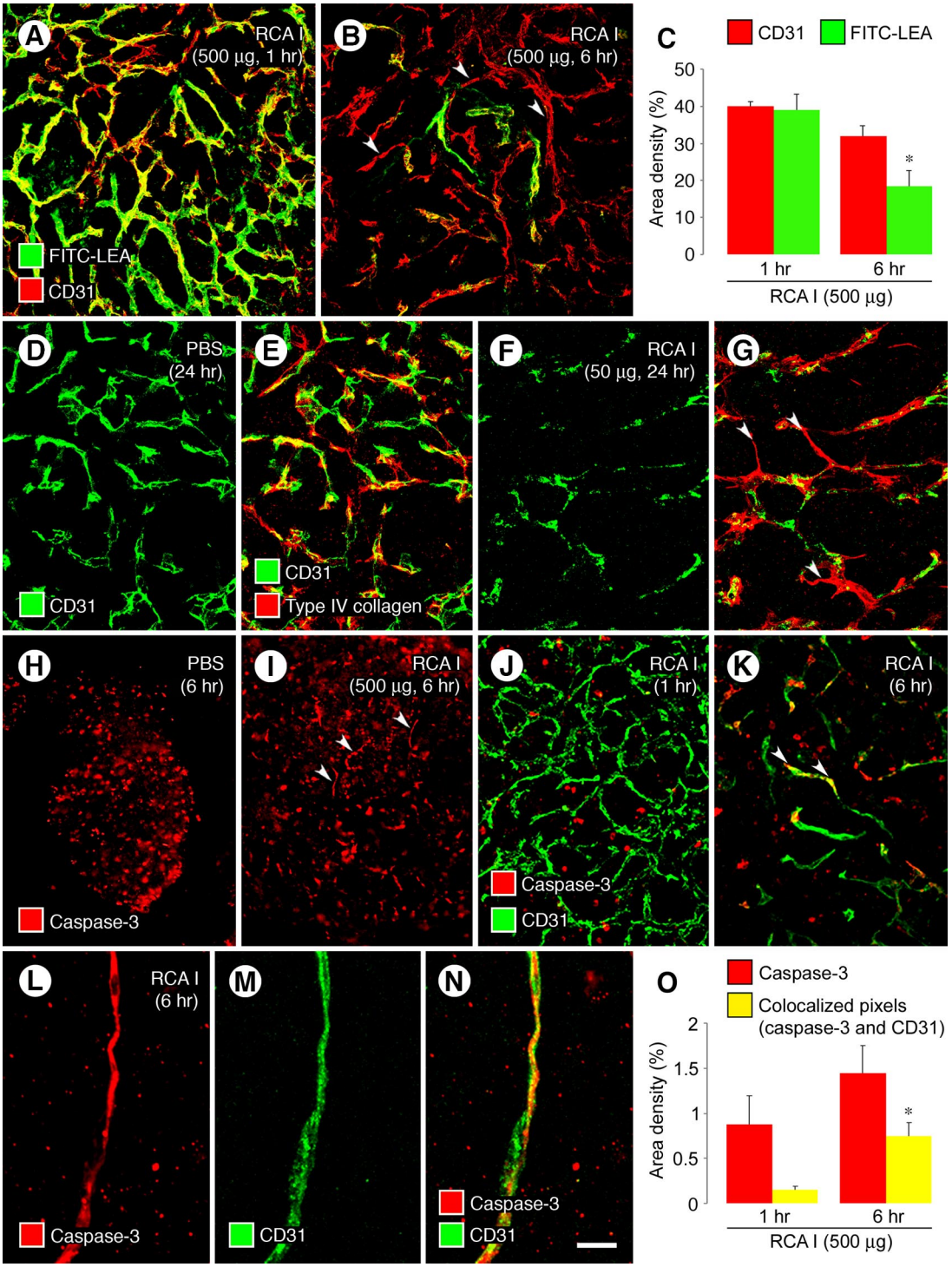


**Figure 6.** Reduced patency, apoptosis, and regression of tumor vessels after RCA I. Confocal micrographs (**A**, **B**) showing that most blood vessels in RIP-Tag2 tumors were stained by FITC-LEA (green) injected i.v. at 1 hour but not at 6 hours after injection of 500 $\mu$g RCA I. However, CD31 (red) staining of tumor vessels was largely normal, indicating that most of the tumor vasculature was still present where FITC-LEA staining was absent at 6 hours (**B**, **arrowheads** mark examples). Measurements (**C**) show 53% reduction in FITC-LEA labeling of tumor vessels between 1 hour and 6 hours after RCA I but only 20% reduction in CD31 staining. Loss of FITC-LEA labeling reflects reduced patency and/or perfusion of blood vessels.[32,33] Confocal micrographs (**D**–**G**) showing similar distributions of CD31 (endothelial cells) and type IV collagen (basement membrane) in RIP-Tag2 tumors at baseline (**D**, **E**) but markedly lower CD31 than type IV collagen at 24 hours after i.v. injection of 50 $\mu$g RCA I, where many tumor vessels had regressed and left behind empty sleeves of basement membrane (**F**, **G**, **arrowheads**). Fluorescence micrographs (**H**, **I**) that illustrate the activated caspase-3 immunofluorescence of round cells in RIP-Tag2 tumors under baseline conditions (**H**) for comparison with scattered curvilinear segments of activated caspase-3 that mark apoptotic endothelial cells present at 6 hours after injection of 500 $\mu$g RCA I (**I**, **arrowheads**). Confocal micrographs (**J**–**N**) comparing tumors after 500 $\mu$g RCA I, where activated caspase-3 immunoreactivity is limited to scattered round cells at 1 hour (**J**), but curvilinear cells that colocalize with CD31, indicative of apoptotic endothelial cells (**arrowheads**), are present at 6 hours (**K**, **L**–**N**). Measurements (**O**) of activated caspase-3 immunofluorescence at 1 and 6 hours after injection of 500 $\mu$g RCA I compare the slight increase in overall activated caspase-3 to the fourfold increase in activated caspase-3 that colocalized with CD31. $^*P < 0.05$ compared with corresponding value in 1 hour group in both graphs. Scale bar in (**N**)**:** 60 $\mu$m (**A**, **B**, **D**–**G**, **J**, **K**); 120 $\mu$m (**H**, **I**); 10 $\mu$m (**L**–**N**).

The increased abundance of "empty" basement membrane sleeves[33] that lacked CD31 staining (Figure 6, D–G) at 24 hours after a 50-$\mu$g dose of RCA I was consistent with the regression of many tumor vessels within this period.

### *Endothelial Cell Apoptosis after RCA I*

Under baseline conditions, cells stained for activated caspase-3 immunoreactivity were abundant in RIP-Tag2 tumors and were invariably round and resembled tumor cells (Figure 6H). However, at 6 hours after injection of 500 $\mu$g RCA I, some activated caspase-3 staining had a vascular pattern, indicative of regressing endothelial cells (Figure 6I, arrowheads). Activated caspase-3 immunoreactivity was not found in the acinar pancreas under these conditions.

Tumor cells stained for activated caspase-3 at 1 hour after RCA I did not colocalize with CD31 staining of tumor blood vessels (Figure 6J), but at 6 hours some activated caspase-3 immunoreactivity was associated with tumor vessels (Figure 6K, arrowheads). This association was confirmed by colocalization of activated caspase-3 staining with CD31 immunoreactivity, indicative of apoptotic endothelial cells in tumor vessels (Figure 6, L–N). The overall amount of activated caspase-3 immunoreactivity in RIP-Tag2 tumors was not significantly greater at 6 hours after RCA I, but the amount that colocalized with CD31 at 6 hours was fourfold the value at 1 hour (Figure 6O).

### *Macrophage Uptake of Endothelial Cell Fragments*

VEGFR-2 staining had a distinct vascular pattern in tumors at 6 minutes or 1 hour after injection of RCA I (Figures 2A and 4A), but at 6 hours most VEGFR-2 immunoreactivity was in form of blobs that colocalized with RCA I (Figure 2, C, H, and I). Some blobs of VEGFR-2 or RCA I appeared to be inside F4/80-positive macrophages (Figure 7, A–D, arrowheads), which was confirmed by isosurface rendering of confocal image stacks and image rotation (Figure 7E, arrowheads), as observed for apoptotic endothelial cells that are ingested by macrophages during vascular remodeling in the eye of mouse embryos.[44,45]

### *Reduction in RCA I Binding after Inhibition of VEGF Signaling*

Further evidence for RCA I binding to tumor vessels through a VEGFR-2-dependent process was sought by exploiting the known decrease in VEGFR-2 expression in tumor vessels that follows inhibition of VEGF signaling.[32,33] In particular, we asked whether RCA I binding was reduced by down-regulation of VEGFR-2 in endothelial cells of RIP-Tag2 tumors after treatment with the VEGF receptor tyrosine kinase inhibitor AG-028262 for 7 days.[32] We found that binding of rhodamine-RCA I to tumor vessels was reduced 88% after this treatment, but tumor vascularity assessed by CD31 staining was reduced by only 36% (Figure 7, F–H). Dot-like RCA I fluorescence in tumor blood vessels was also significantly reduced after AG-028262 for 7 days (Figure 7, I–J). Similarly, tumors treated with AG-028262 for 7 days did not have curvilinear (vascular) staining of activated caspase-3 at 6 hours after RCA I (Figure 7K), unlike tumors that were not treated with the inhibitor (Figure 6I).

## *Discussion*

This study examined the selectivity and the functional consequences of RCA I binding to endothelial cells of blood vessels of tumors. We found that rhodamine-RCA I injected i.v. bound rapidly and preferentially to the vasculature of RIP-Tag2 tumors. RCA I initially had a diffuse distribution on the lumen of tumor vessels but at 1 hour had a dot-like pattern, reflecting internalization by endothelial cells. VEGFR-2 immunofluorescence also had a dot-like pattern and partially colocalized with RCA I, but was reduced by 95% at 6 hours after injection of RCA I. Some tumor vessel endothelial cells underwent apoptosis. By 24 hours some vessels regressed, and empty basement membrane sleeves were present.

Our observations of the internalization of RCA I by endothelial cells of tumor vessels *in vivo* are consistent with reports of RCA I binding and sequestration by endothelial cells in culture and *in vivo*.[29,46] Binding and internalization of $^{125}$I-RCA I by brain microvascular endothelial cells *in vitro* at 37°C have half-lives of 5 minutes and 14 minutes, respectively.[46] Binding to glycoconjugates in caveolae gives RCA I a subtly punctate pattern even at 4°C, along with uniform binding over the cell surface.[46] Ultrastructural studies have shown that RCA I is internalized into coated and uncoated vesicles, endosomes, and the trans-Golgi network.[29,46]

Several lines of evidence indicate that RCA I shares the endocytic pathway of VEGFR-2 in endothelial cells: (i) RCA I colocalized with VEGFR-2 immunoreactivity in endosomes in endothelial cells of tumor vessels. (ii) VEGFR-2 rapidly decreased in endothelial cells of tumor vessels after injection of RCA I, and this reduction was significantly greater than corresponding changes in other endothelial membrane proteins (VEGFR-3, CD31, CD105). (iii) Biotinylated RCA I in avidin precipitants of tumor homogenates was labeled by anti-VEGFR-2 antibody in Western blots, consistent with the presence of VEGFR-2 in RCA I-bound protein complexes. (iv) Reduction in VEGFR-2 expression after treatment with AG-028262 for 7 days led to reduced RCA I binding and internalization into endothelial cells of tumor vessels.[32,33] Pretreatment with AG-028262 also prevented the massive endothelial cell apoptosis that was present 6 hours after injection of RCA I. Although RCA I does not bind exclusively to VEGFR-2, the exaggerated expression of these receptors on tumor vessels may contribute to the impact of the lectin on tumor vasculature.

VEGFR-2 immunoreactivity of tumor blood vessels rapidly decreased in a dose- and time- dependent manner

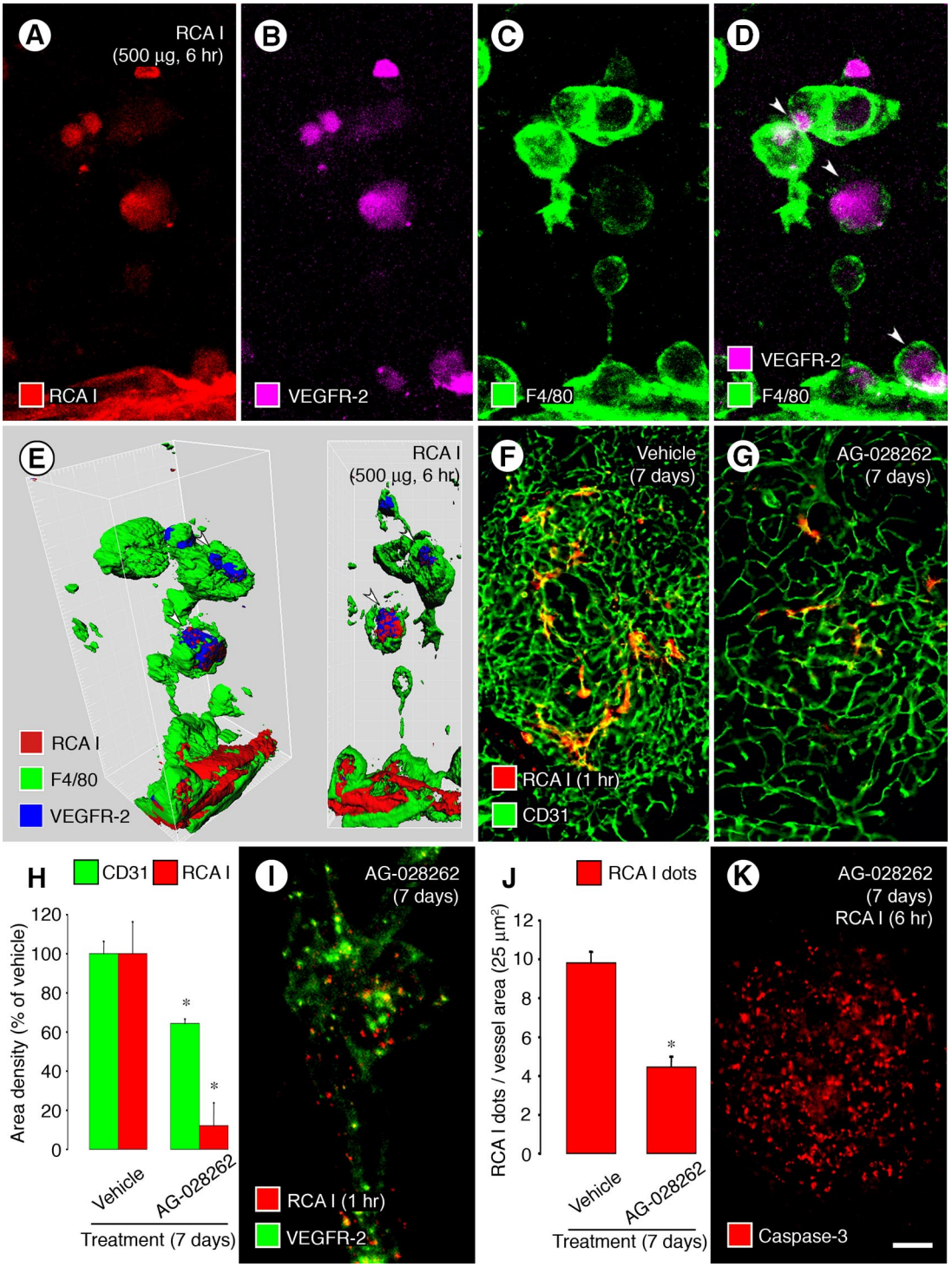


**Figure 7.** Internalization of RCA I and VEGFR-2: Macrophage engulfment and effects of VEGFR inhibition by AG-028262. Confocal micrographs showing blobs of RCA I colocalized with VEGFR-2 immunoreactivity in RIP-Tag2 tumors at 6 hours after injection of 500 $\mu$g RCA I (**A**–**B**). Some of the blobs are inside F4/80-positive macrophages (**C**, **D**, **arrowheads**). Isosurface rendering of confocal stack images confirmed that the blobs were within F4/80-positive cells (**E, arrowheads**). Fluorescence micrographs (**F**, **G**) comparing the abundant RCA I binding to tumor vessels at 1 hour after injection under baseline conditions (**F**) to little RCA I binding in tumors treated with AG-028262 (80 mg/kg) for 7 days (**G**). Measurements (**H**) showing greater reduction in RCA I fluorescence than in tumor vascularity assessed by CD31 staining after treatment with AG-028262 for 7 days. Confocal micrograph and graph (**I**, **J**) of dot-like RCA I fluorescence (500 $\mu$g, 1 hour) showing the reduction by treatment with AG-028262 for 7 days before the injection of RCA I. Fluorescence micrograph (**K**) of activated caspase-3 immunoreactivity showing round cell staining (tumor cells), but little or no curvilinear staining (endothelial cells), in a tumor treated for 7 days with AG-028262 and then prepared 6 hours after injection of RCA I (compare with Figure 6I). $^*P < 0.05$ compared with vehicle group in both graphs. Scale bar in (**K**)**:** 10 $\mu$m (**A**–**E**, **I**); 120 $\mu$m (**F**, **G**, **K**).

after injection of RCA I. The reduction in VEGFR-2 was much greater on tumor vessels than on normal blood vessels. The VEGFR-2 reduction of 95% in endothelial cells of tumor vessels at 6 hours was significantly greater than the 21% to 33% reductions in VEGFR-3, CD31, and CD105. The much more rapid and severe reduction of VEGFR-2 could be explained by preferential effects of RCA I on VEGFR-2 expression or on the high turnover of VEGFR-2 associated with its importance in signaling for growth and survival of endothelial cells in tumor vessels.[42,43] Alternatively, if RCA I triggers release of VEGF from tumor cells, ligand binding could lead to VEGFR-2 internalization in endothelial cells, but we observed no evidence of RCA I uptake by tumor cells. Inhibition of protein synthesis by RCA I A chain internalized into endothelial cells would also contribute to the reduction in VEGFR-2.[12,13]

Down-regulation of VEGFR-2 after binding and internalization of RCA I was followed by loss of patency and cessation of blood flow. Some endothelial cells of tumor vessels underwent apoptosis, as documented by the appearance of activated caspase-3 staining that colocalized with CD31. Apoptosis of endothelial cells could result from protein synthesis inhibition, inhibition of integrins, or other toxic actions of A chains of internalized RCA I, as indicated by multiple mechanisms of endothelial cell death mediated by ricin.[27,47] Tumor vessels that regressed after RCA I left behind empty sleeves of basement membrane, as found in the same tumor model after inhibition of VEGF signaling.[32–34]

The appearance of blobs that had RCA I fluorescence and VEGFR-2 immunoreactivity within F4/80-positive macrophages indicates a fate of some apoptotic endothelial cells of regressing tumor vessels in this model. Macrophages are known to phagocytize apoptotic endothelial cells of blood vessels undergoing remodeling or regression.[44,45,48]

RIP-Tag2 tumors have high strong VEGF immunoreactivity in tumor cells.[49,50] VEGF immunoreactivity associated with tumor blood vessels had a distinctive dot-like pattern, as previously reported in endothelial cells *in vitro*.[39–42] Much of the dot-like VEGF fluorescence colocalized with VEGFR-2, indicative of VEGF/VEGFR-2 complexes internalized into the endothelial cells. Despite its close association with VEGFR-2, RCA I fluorescence did not colocalize with VEGF in endothelial cells of tumor vessels. This finding makes it unlikely that RCA I primarily binds to VEGF or VEGF/VEGFR-2 complexes instead of to VEGFR-2 itself or to protein complexes that contain the receptor.

Yet to be determined is whether the regression of tumor vessels after i.v. administration of RCA I would lead to slowed tumor growth. We attempted to address this issue but found that RCA I doses of 25 $\mu$g or larger had lethal effects in RIP-Tag2 mice within 24 hours. The $LD_{50}$ of RCA I was calculated to be 1.23 mg/kg in RIP-Tag2 mice, which is in the range reported previously.[18]

The preferential binding of RCA I to endothelial cells of tumor vessels indicates its potential as probe for targeting diagnostics or therapeutics to the tumor vasculature. Although it is still unknown whether this property applies uniformly to different types of tumors, the present results are consistent with reports for other preclinical tumor models.[28] Use of intact RCA I may be limited by the toxicity, which is partly due to the inhibitory activity of RCA I A chains on protein synthesis. We did not observe immediate toxicity associated with the hemagglutinin properties of RCA I. However, if recombinant B chains of RCA I have the same tumor targeting properties as the intact lectin, they could be conjugated to anti-angiogenic agents or other therapeutics to increase the efficiency and selectivity of drug delivery to tumor vessels. More detailed information about the endothelial cell glycoconjugates that bind RCA I should help to achieve this.

We conclude that RCA I rapidly and preferentially binds to and is internalized by endothelial cells of RIP-Tag2 tumors. After internalization, RCA I leads to striking reduction of endothelial cell VEGFR-2 expression in a dose- and time-dependent manner. The reduction of VEGFR-2 is accompanied by endothelial cell apoptosis, loss of vessel patency, and tumor vessel regression. Treatment with an inhibitor of VEGF signaling reduces RCA I binding as a feature of vessel normalization. Overall, these studies demonstrate the profound effect of RCA I on tumor blood vessels, with an especially large impact on VEGFR-2, and raise the possibility of use of galactose-binding B chains of RCA I for targeted delivery to tumor blood vessels.

## *Acknowledgments*

We thank Pfizer for supplying AG-028262, Rolf Brekken for generously providing the anti-VEGFR-2 antibody, and Mimi Zeiger for editing the manuscript. We also thank Beverly Falcón, Hiroya Hashizume, Jeyling Chou, Peter Baluk, and Tatsuma Okazaki for their valuable advice and discussion.

## *References*

1. Baluk P, Hashizume H, McDonald DM: Cellular abnormalities of blood vessels as targets in cancer. Curr Opin Genet Dev 2005, 15:102–111
2. McDonald DM, Baluk P: Significance of blood vessel leakiness in cancer. Cancer Res 2002, 62:5381–5385
3. Fukumura D, Jain RK: Imaging angiogenesis and the microenvironment. APMIS 2008, 116:695–715
4. Nishida S, Akai F, Hiruma S, Maeda M, Tanji K, Hashimoto S: Experimental study of WGA binding on the endothelial cell surface in cerebral ischemia. Histol Histopathol 1986, 1:69–74
5. Jackson CJ, Garbett PK, Nissen B, Schrieber L: Binding of human endothelium to Ulex europaeus I-coated Dynabeads: application to the isolation of microvascular endothelium. J Cell Sci 1990, 96:257–262
6. Augustin-Voss HG, Pauli BU: Migrating endothelial cells are distinctly hyperglycosylated and express specific migration-associated cell surface glycoproteins. J Cell Biol 1992, 119:483–491
7. Thurston G, Baluk P, Hirata A, McDonald DM: Permeability-related changes revealed at endothelial cell borders in inflamed venules by lectin binding. Am J Physiol 1996, 271:H2547–H2562
8. Porter GA, Palade GE, Milici AJ: Differential binding of the lectins Griffonia simplicifolia I and Lycopersicon esculentum to microvascular endothelium: organ-specific localization and partial glycoprotein characterization. Eur J Cell Biol 1990, 51:85–95
9. Lugnier A, Dirheimer G: Differences between ricin and phytohemagglutinins from Ricinus communis seeds. FEBS Lett 1973, 35:117–120
10. Lin TT, Li SL: Purification and physicochemical properties of ricins

and agglutinins from Ricinus communis. Eur J Biochem 1980, 105:453–459
11. Goldstein IJ, Poretz RD: Isolation, physicochemical characterization, and carbohydrate-binding specificity of lectins. Edited by IE Liener, N Sharon, IJ Goldstein. Orlando FL, Academic Press, Inc., 1986, pp. 35–247
12. Barbieri L, Ciani M, Girbes T, Liu WY, Van Damme EJ, Peumans WJ, Stirpe F: Enzymatic activity of toxic and non-toxic type 2 ribosome-inactivating proteins. FEBS Lett 2004, 563:219–222
13. Audi J, Belson M, Patel M, Schier J, Osterloh J: Ricin poisoning: a comprehensive review. JAMA 2005, 294:2342–2351
14. Ohnaka K, Nishikawa M, Takayanagi R, Haji M, Nawata H: Partial purification of phosphoramidon-sensitive endothelin converting enzyme in porcine aortic endothelial cells: high affinity for Ricinus communis agglutinin. Biochem Biophys Res Commun 1992, 185:611–616
15. Brech A, Magnusson S, Stang E, Berg T, Roos N: Receptor-mediated endocytosis of ricin in rat liver endothelial cells. An immunocytochemical study. Eur J Cell Biol 1993, 60:154–162
16. Magnusson S, Kjeken R, Berg T: Characterization of two distinct pathways of endocytosis of ricin by rat liver endothelial cells. Exp Cell Res 1993, 205:118–125
17. Lin JY, Liu SY: Studies on the antitumor lectins isolated from the seeds of Ricinus communis (castor bean). Toxicon 1986, 24:757–765
18. Zhan J, Zhou P: A simplified method to evaluate the acute toxicity of ricin and ricinus agglutinin. Toxicology 2003, 186:119–123
19. Fodstad O, Kvalheim G, Godal A, Lotsberg J, Aamdal S, Host H, Pihl A: Phase I study of the plant protein ricin. Cancer Res 1984, 44:862–865
20. Shah SA, Halloran PM, Ferris CA, Levine BA, Bourret LA, Goldmacher VS, Blattler WA: Anti-B4-blocked ricin immunotoxin shows therapeutic efficacy in four different SCID mouse tumor models. Cancer Res 1993, 53:1360–1367
21. Calvete JA, Newell DR, Wright AF, Rose MS: In vitro and in vivo antitumor activity of ZENECA ZD0490, a recombinant ricin A-chain immunotoxin for the treatment of colorectal cancer. Cancer Res 1994, 54:4684–4690
22. Schnell R, Katouzi AA, Linnartz C, Schoen G, Drillich S, Hansmann ML, Schiefer D, Barth S, Zangemeister-Wittke U, Stahel RA, Diehl V, Engert A: Potent anti-tumor effects of an anti-CD24 ricin A-chain immunotoxin in vitro and in a disseminated human Burkitt's lymphoma model in SCID mice. Int J Cancer 1996, 66:526–531
23. Fidias P, Grossbard M, Lynch TJ, Jr.: A phase II study of the immunotoxin N901-blocked ricin in small-cell lung cancer. Clin Lung Cancer 2002, 3:219–222
24. Soler-Rodriguez AM, Ghetie MA, Oppenheimer-Marks N, Uhr JW, Vitetta ES: Ricin A-chain and ricin A-chain immunotoxins rapidly damage human endothelial cells: implications for vascular leak syndrome. Exp Cell Res 1993, 206:227–234
25. Lindstrom AL, Erlandsen SL, Kersey JH, Pennell CA: An in vitro model for toxin-mediated vascular leak syndrome: ricin toxin A chain increases the permeability of human endothelial cell monolayers. Blood 1997, 90:2323–2334
26. Baluna R, Rizo J, Gordon BE, Ghetie V, Vitetta ES: Evidence for a structural motif in toxins and interleukin-2 that may be responsible for binding to endothelial cells and initiating vascular leak syndrome. Proc Natl Acad Sci USA 1999, 96:3957–3962
27. Baluna R, Coleman E, Jones C, Ghetie V, Vitetta ES: The effect of a monoclonal antibody coupled to ricin A chain-derived peptides on endothelial cells in vitro: insights into toxin-mediated vascular damage. Exp Cell Res 2000, 258:417–424
28. Hunter F, Xie J, Trimble C, Bur M, Li KC: Rhodamine-RCA in vivo labeling guided laser capture microdissection of cancer functional angiogenic vessels in a murine squamous cell carcinoma mouse model. Mol Cancer 2006, 5:5
29. Nakamura-Ishizu A, Morikawa S, Shimizu K, Ezaki T: Characterization of sinusoidal endothelial cells of the liver and bone marrow using an intravital lectin injection method. J Mol Histol 2008, 39:471–479
30. Debbage PL, Griebel J, Ried M, Gneiting T, DeVries A, Hutzler P: Lectin intravital perfusion studies in tumor-bearing mice: micrometer-resolution, wide-area mapping of microvascular labeling, distinguishing efficiently and inefficiently perfused microregions in the tumor. J Histochem Cytochem 1998, 46:627–639
31. Hanahan D: Heritable formation of pancreatic beta-cell tumours in transgenic mice expressing recombinant insulin/simian virus 40 oncogenes. Nature 1985, 315:115–122
32. Mancuso MR, Davis R, Norberg SM, O'Brien S, Sennino B, Nakahara T, Yao VJ, Inai T, Brooks P, Freimark B, Shalinsky DR, Hu-Lowe DD, McDonald DM: Rapid vascular regrowth in tumors after reversal of VEGF inhibition. J Clin Invest 2006, 116:2610–2621
33. Inai T, Mancuso M, Hashizume H, Baffert F, Haskell A, Baluk P, Hu-Lowe DD, Shalinsky DR, Thurston G, Yancopoulos GD, McDonald DM: Inhibition of vascular endothelial growth factor (VEGF) signaling in cancer causes loss of endothelial fenestrations, regression of tumor vessels, and appearance of basement membrane ghosts. Am J Pathol 2004, 165:35–52
34. Nakahara T, Norberg SM, Shalinsky DR, Hu-Lowe DD, McDonald DM: Effect of inhibition of vascular endothelial growth factor signaling on distribution of extravasated antibodies in tumors. Cancer Res 2006, 66:1434–1445
35. Argmann CA, Auwerx J: Collection of blood and plasma from the mouse. Curr Protoc Mol Biol 2006, Chapter 29:Unit 29A 23
36. Riches AC, Sharp JG, Thomas DB, Smith SV: Blood volume determination in the mouse. J Physiol 1973, 228:279–284
37. Mitruka BM, Rawnsley HM: Clinical, biochemical and hematological reference values in normal experimental animals and normal humans. Masson Publishing 1981, pp9–12
38. Baluk P, Fuxe J, Hashizume H, Romano T, Lashnits E, Butz S, Vestweber D, Corada M, Molendini C, Dejana E, McDonald DM: Functionally specialized junctions between endothelial cells of lymphatic vessels. J Exp Med 2007, 204:2349–2362
39. Wang D, Lehman RE, Donner DB, Matli MR, Warren RS, Welton ML: Expression and endocytosis of VEGF and its receptors in human colonic vascular endothelial cells. Am J Physiol Gastrointest Liver Physiol 2002, 282:G1088–G1096
40. Bhattacharya R, Kang-Decker N, Hughes DA, Mukherjee P, Shah V, McNiven MA, Mukhopadhyay D: Regulatory role of dynamin-2 in VEGFR-2/KDR-mediated endothelial signaling. FASEB J 2005, 19:1692–1694
41. Lampugnani MG, Orsenigo F, Gagliani MC, Tacchetti C, Dejana E: Vascular endothelial cadherin controls VEGFR-2 internalization and signaling from intracellular compartments. J Cell Biol 2006, 174:593–604
42. Santos SC, Miguel C, Domingues I, Calado A, Zhu Z, Wu Y, Dias S: VEGF and VEGFR-2 (KDR) internalization is required for endothelial recovery during wound healing. Exp Cell Res 2007, 313:1561–1574
43. Shaheen RM, Tseng WW, Vellagas R, Liu W, Ahmad SA, Jung YD, Reinmuth N, Drazan KE, Bucana CD, Hicklin DJ, Ellis LM: Effects of an antibody to vascular endothelial growth factor receptor-2 on survival, tumor vascularity, and apoptosis in a murine model of colon carcinomatosis. Int J Oncol 2001, 18:221–226
44. Mitchell CA, Risau W, Drexler HC: Regression of vessels in the tunica vasculosa lentis is initiated by coordinated endothelial apoptosis: a role for vascular endothelial growth factor as a survival factor for endothelium. Dev Dyn 1998, 213:322–333
45. Lobov IB, Rao S, Carroll TJ, Vallance JE, Ito M, Ondr JK, Kurup S, Glass DA, Patel MS, Shu W, Morrisey EE, McMahon AP, Karsenty G, Lang RA: WNT7b mediates macrophage-induced programmed cell death in patterning of the vasculature. Nature 2005, 437:417–421
46. Raub TJ, Audus KL: Adsorptive endocytosis and membrane recycling by cultured primary bovine brain microvessel endothelial cell monolayers. J Cell Sci 1990, 97 (Pt 1):127–138
47. Brigotti M, Alfieri R, Sestili P, Bonelli M, Petronini PG, Guidarelli A, Barbieri L, Stirpe F, Sperti S: Damage to nuclear DNA induced by Shiga toxin 1 and ricin in human endothelial cells. FASEB J 2002, 16:365–372
48. Williams JM, Colman R, Brookes CJ, Savage CO, Harper L: Anti-endothelial cell antibodies from lupus patients bind to apoptotic endothelial cells promoting macrophage phagocytosis but do not induce apoptosis. Rheumatology (Oxford) 2005, 44:879–884
49. Christofori G, Naik P, Hanahan D: Vascular endothelial growth factor and its receptors, flt-1 and flk-1, are expressed in normal pancreatic islets and throughout islet cell tumorigenesis. Mol Endocrinol 1995, 9:1760–1770
50. Inoue M, Hager JH, Ferrara N, Gerber HP, Hanahan D: VEGF-A has a critical, nonredundant role in angiogenic switching and pancreatic beta cell carcinogenesis. Cancer Cell 2002, 1:193–202